Bulletin of Engineering Geology and the Environment (2019) 78:6221–6234
https://doi.org/10.1007/s10064-019-01499-x

ORIGINAL PAPER

Ground load on tunnels built using new Austrian tunneling method: study of a tunnel passing through highly weathered sandstone

Ben-Guo He [1,2] · Xi-Wei Zhang [1] · Hong-Pu Li [1]

Received: 18 October 2018 / Accepted: 2 March 2019 / Published online: 14 March 2019

Abstract

The ground load acting on a tunnel is an important issue in tunnel design, especially when the tunnel passes through highly weathered sandstone. A systematic field-monitoring campaign was performed to investigate the ground loads on a tunnel structure, the behavior of the composite support system, and the deformation of the tunnel boundaries. The monitoring results were analyzed and compared with those of various theories, such as the whole-soil column theory and those of Terzaghi, Bierbaumer, Xie Jiaxiu, and Protodyakonov. The ground load on a highway tunnel in highly weathered sandstone does not conform to current theoretical methodologies. It was confirmed that Terzaghi's theory is suitable for estimating the peak magnitude of the vertical ground load, but differs from the field-monitoring results for ground load distribution profile. To facilitate tunnel design, a potential profile for ground loads is proposed, in which the vertical load component is 'mountain'-shaped and the horizontal component adopts a 'folded-line' pattern. The roof rockbolts are subjected to compression and should be replaced by pipe grouting that is capable of providing enhanced reinforcement and accelerating the construction schedule. The bending moments acting on the lining were found to form a 'butterfly' shape. Supplementary finite-element modeling was undertaken to explore the mechanical behavior of the tunnel lining. These results indicated that steel rebar needs to be pre-installed in both the intrados of the lining roof and extrados of the spandrels to improve the lining tensile strength.

Keywords Highway tunnel · Ground load · Weathered sandstone · Field monitoring · Lining

Introduction

The determination of ground loads acting on tunnel structures is one of the most complex issues in deep excavation science. This typically involves deriving parameters for the composite support system (Kim et al. 2015; Singh et al. 1997) as well as assessing risks posed to underground safety in the event that the ground load exceeds the bearing capacity of the tunnel structure. It is widely held that the performance of the composite support system of the tunnel (that is, the primary support and concrete lining) depends on the post-excavation ground load (Goel et al. 1996; Simanjuntak et al. 2014). This is true for tunneling through highly weathered sandstone, which is typically characterized by softness and dense discontinuities, giving rise to difficult challenges for safe construction. As might be expected, obtaining appropriate information about ground loads helps to facilitate a safer and more economical tunnel design (Gurocak 2011).

Most methodologies for predicting ground loads on tunnels built using the New Austrian Tunneling Method (NATM; Rabcewicz 1964) depend, to some extent, upon taking an empirical approach to the problem, such as in the whole-soil column theory and those of Terzaghi (1946), Bierbaumer (1913), Xie Jiaxiu (China Railway Eryuan Engineering Group 1997; Song et al. 2007), and Protodyakonov (Szechy 1970). In these theories, the ground loads are assumed to be uniform in the vertical component and right-angled trapezoid in the horizontal component. Realistic ground loads on a tunnel structure may, however, not have these ideal distributions, which significantly affects its design parameters. To date, the resultant differences between existing theoretical solutions have not been compared or discussed with respect to

✉ Ben-Guo He
hebenguo@mail.neu.edu.cn

[1] Key Laboratory of Ministry of Education on Safe Mining of Deep Metal Mines, Northeastern University, Shenyang 110819, China

[2] Department of Geological and Environmental Sciences, Ben-Gurion University of the Negev, 84105 Beer Sheva, Israel

Fig. 1 Map showing the location of Piaoli Tunnel in southwest China

specific engineering applications. When tunneling in highly weathered sandstone with softness and density discontinuities, selection of rockbolts of identical length may be not reasonable. Carrying out a structural analysis of the tunnel lining is therefore an essential practice for a tunnel passing through such material.

(a)

(b)

Fig. 2 Highly weathered sandstone encountered at Chainage YK6 + 955: (a) outcrop at the working face of the tunnel; (b) an enlarged view (Photographs by Dr. Ben-Guo He)

The first report on vertical ground loads was provided by Bierbaumer (1913), and included various variables of relevance (including unit density, internal friction, cohesion of the medium, and excavation span). Later, in his book, *Theoretical Soil Mechanics*, Terzaghi (1943) initially proposed the concept of 'arching' in an attempt to evaluate whether or not a tunnel is stable. Terzaghi (1946) then developed an empirical equation based on data from a collection of railway tunnels constructed in the eastern Alps where rock mass quality was classified into nine categories; the pressure on the tunnel structures was assumed to be uniform.

Barton et al. (1974) proposed a method for calculating ground load that took into account the presence of joint sets, but did not consider the dimensions of the opening space. More recently, roof settlement observed via field monitoring was used in conjunction with back analysis to estimate the ground load imposed on a two-lane highway tunnel in Korea (Kim et al. 2015). However, this method could not be used to provide a potential profile shape for the ground load in the vertical and horizontal directions. Using the three-dimensional finite-difference method, FLAC^{3D}, Rolf et al. (2009) studied a variety of loads acting on the Gotthard Base Tunnel in Switzerland and compared the results with field-monitoring data in an attempt to achieve a profile of the ground load. Field-monitoring technology was also applied to an underground excavation passing through loess (Zhang et al. 2013); the ground pressure between the primary support and

Table 1 Mechanical parameters for highly weathered sandstone of Piaoli highway tunnel

Unit density, γ (kN m^{-3})	Cohesion, c (kPa)	Friction angle, φ (°)	Poisson's ratio, υ	Young's modulus, E (GPa)	Initial stress ratio, K*
22	200	35	0.31	3.2	0.48

*Note: K denotes the ratio of in-situ horizontal to vertical stress

the loess was significantly incompatible with the loosening ground pressure prescribed by theoretical solutions.

All of these aforementioned methods, aimed at predicting the ground load, focus on the vertical ground pressure on a tunnel structure σ_v, but often ignore the horizontal pressure σ_h. Moreover, the various methods can give rise to strikingly different results when predicting the ground load for a specific scenario (Taromi et al. 2017). To date, this issue, surprisingly, has not been studied very thoroughly and is particularly troublesome in highly weathered sandstone, which is widely distributed around the world (Alija et al. 2014).

The purpose of this study was to explore the effect of non-squeezing ground loads on the structure of the Piaoli Tunnel, a two-lane span embedded in highly weathered sandstone in Qiannan Autonomous Prefecture, Guizhou Province, China (Fig. 1). The geological properties here are typical of those encountered in southwest China. Systematic field-monitoring experiments were devised to derive a realistic representation of the ground loads acting on the tunnel structure, internal forces acting on the cast-in-place reinforced lining, axial forces acting on the rockbolts, and evolution of the deformation of the tunnel boundaries. In addition, finite-element numerical modeling was implemented to examine the mechanical behavior of the tunnel lining. Our results should provide a meaningful way of designing the support needed in a deep two-lane highway tunnel.

Systematic field-monitoring preparation

Brief introduction to the tunnel

Piaoli highway tunnel is located in Qiannan Autonomous Prefecture, Guizhou Province, in southwest China. It has a total length upwards of 885 m and overburden depth of 86–120 m. In terms of both laboratory and field observations, most of the rock mass consists of non-squeezing, highly weathered sandstone (Fig. 2). More specifically, it has a rock mass rating ranging from 'poor' to 'fair' (Bieniawski 1973). The tunnel has a horseshoe-shaped cross-section with an opening span of 12.6 m, height of 9.8 m, and excavated area of 94.6 m^2.

Considering the in-situ observations of outcrops at the working face of the tunnel, as well as field geological survey reports, the mechanical parameters of the highly weathered sandstone are summarized in Table 1 and used throughout this section. The field observations are recorded as Classification no. V using the Chinese rock mass classification system (JTG D70-2004 2004); they can readily be converted to geological strength index (GSI) values (Hatzor et al. 2017; Hoek and Brown 1997) using Table 2.

After tunneling and removal of the rubble, primary support was employed (rockbolts, steel ribs, and flexible shotcrete spraying) according to the practices commonly used in composite support procedures for tunnels constructed using the NATM (Hjálmarsson 2011). When deformation of the primary support stabilized, a waterproof layer and cast-in-place

Table 2 Correlation between global strength index (GSI) values and rock mass classification used in China

"GSI" method	≥ 81	80~61	60~41	40~21	< 21
Chinese rock mass classification	I	II	III	IV	V	VI

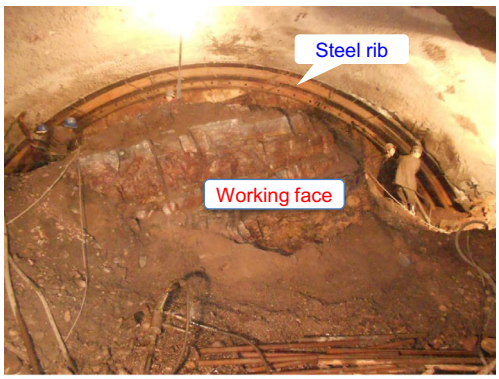

(a)

(b)

Fig. 3 Steel ribs installed as part of the primary support applied during tunneling: (a) installation of steel ribs after tunneling excavation; (b) an enlarged view of the steel ribs

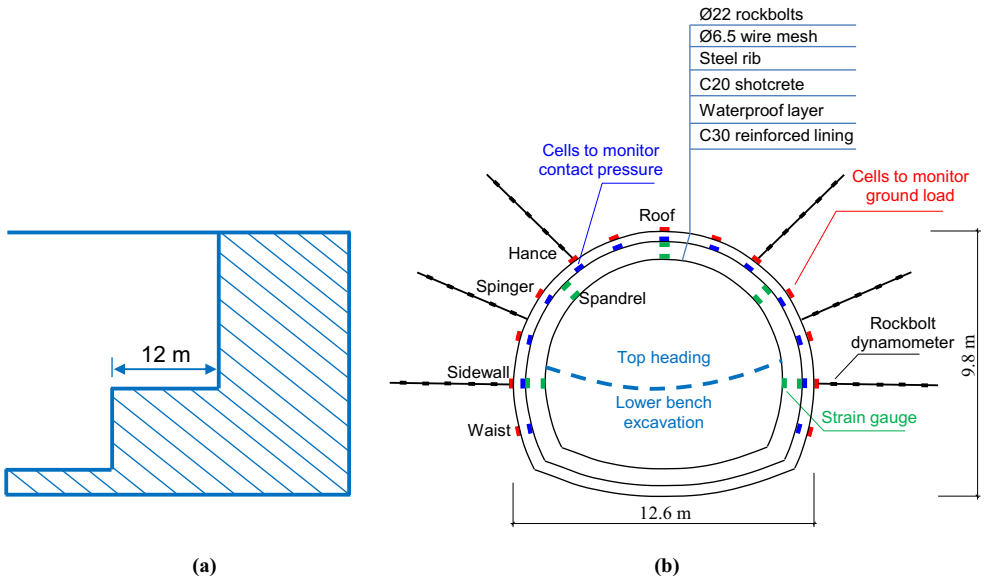

Fig. 4 Schematic diagram of two-lane highway tunnel cross-section: (a) top heading and bench excavation method employed; (b) layout of monitoring instrumentation installed. Note that 'ground load' refers to the load between the highly weathered sandstone and the primary support; 'contact pressure' is the radial stress between the primary support and tunnel lining

concrete lining were applied in accordance with current tunnel design practice (Zhang et al. 2013). The parameters of the composite support system used in the Piaoli tunnel were as follows: (I) ⌀ 22 mm rockbolts of length $L = 4.5$ m and spacing of $S = 1.0$ m (longitudinal direction) × 1.2 m (hoop direction); (II) an advance step of 1 m, equal to the spacing of the steel ribs (Fig. 3), which were required to be welded onto struts at the bottom to ensure that the ribs were capable of bearing a high ground load in the highly weathered sandstone; (III) ⌀ 6.5 mm wire mesh with spaces of 25 cm × 25 cm to prevent ground deterioration in the event of collapse; (IV) 16 cm-thick sprayed C20 shotcrete to complete the primary support; (V) a waterproof layer covering the shotcrete; and finally, (VI) a cast-in-place C30 concrete lining of non-uniform thickness, implemented at a distance 4D from the working face after the tunnel closure stabilized (where D is the opening span).

Monitoring program

To quantitatively assess the non-squeezing ground load acting on a large cross-section of the deep Piaoli highway tunnel, we monitored two sections, YK6 + 955 and YK6 + 960, as our domain of interest (with depths in the range 103–110 m). It should be noted that squeezing ground conditions are beyond the scope of this study. Probing the outcrop of the tunnel working face highlighted the presence of the highly weathered sandstone commonly encountered in southwest China. It is characterized by its fragmented structure and poor condition, i.e., occurrence of numerous joints, fissures, and even structural planes. If a system of structural support is not promptly constructed, the stability of the tunnel gradually deteriorates and it then becomes susceptible to rock spalling and even collapse.

NATM was used here, i.e., the top heading and lower bench were sequentially excavated using a tunneling excavator (Fig. 4a). To explore the ground load acting on the tunnel structure, together with the behavior of the composite support system, we adopted the instrumentation layout shown in Fig. 4b. Following excavation, steel ribs spaced at 1 m and rockbolt dynamometers were installed. Wire mesh (⌀ 6.5 mm) spaced at 25 cm × 25 cm was then welded onto the steel ribs to prevent further ground deterioration in the event of collapse. Ground pressure cells were positioned between the highly weathered sandstone and primary support prior to the spraying of shot concrete (see Fig. 5a-b). After completion of the waterproof layer, contact pressure cells and strain gauges were positioned at the lining steel bars. Finally, concrete was cast through the steel formwork to form the tunnel lining (Fig. 5c). All instrumentation was supplied and calibrated by Yongshun Testing Company (Dandong, China); the testing errors were found to be less than 1%. The electrical connections carrying the data from the measurement instruments were channeled through the tunnel lining. The monitoring signals thus were recorded using secondary instrumentation and used for long-term monitoring.

Behavior of tunnel composite support system

Distribution of ground load

As a fundamental factor in the design of the tunnel structure, ground loads prominently affect the behavior of the structure and, to some extent, the cost of construction process. The ground load acting on the primary support was obtained using

(a)

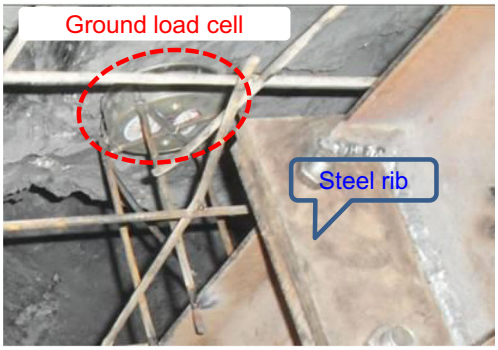

(b)

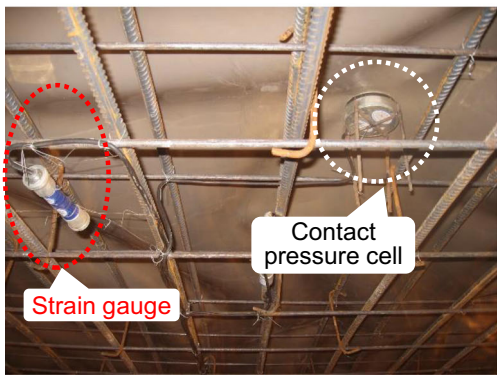

(c)

Fig. 5 Instrumentation used to monitor radial compressive loads acting on the primary support and tunnel lining: (a) preparing the vibrating wire load cells and electrical cables; (b) a ground load cell positioned at a steel rib to monitor the radial ground load between the sandstone and primary support; and (c) a contact pressure cell in place against the primary support and strain gauge fixed to a steel rebar prior to the construction of the cast-in-place lining

ground load cells, which gave the results presented in Fig. 6. In this figure, the label 'failure' near the left springer of Chainage YK6 + 960 means that the ground load cell at this position did not work properly after construction.

As can be appreciated from inspection of Fig. 6, the maximum pressure appeared near the roof of the tunnel at both locations YK6 + 955 and YK6 + 960 (and was roughly double that experienced at the sidewalls). Asynchronous construction is typically involved (e.g., during excavation of the right and left laterals of the lower bench in the NATM), which may account for the asymmetric ground loads acting on the tunnel structure.

From the viewpoint of tunnel design, we sought to establish, as far as possible, the profile of the ground load exerted on deep tunnels with a large cross-section in highly weathered sandstone. To help elucidate the shape of the ground load profile, the radial ground loads monitored at Chainages YK6 + 955 and YK6 + 960 (Fig. 6) were decomposed into their vertical and horizontal components (see Table 3). To simplify the analysis for design practice, a profile was proposed that is typical of this symmetrical and piecewise linear characteristic. Here, the vertical pressure was 'mountain'-shaped (Fig. 7a), i.e., the maximum vertical load (q = 331 kPa, according to Table 3) occurred at the roof of the tunnel. It then dropped linearly to $0.6q$ at the hances of the tunnel and remained constant towards the sidewalls. Similarly, the horizontal load component was described as a 'folded-line' (Fig. 7b). The horizontal load was equal to $0.2q$ at the hance and increased linearly up to $0.5q$ at the sidewalls (leveling off at a point inclined at 72° to the vertical dashed line marking the center of the opening cross-section). The load remained constant until it reached the tunnel invert.

The contact pressure between the primary support and lining directly influences the magnitudes of the thrust N and bending M experienced by the tunnel lining. In terms of numerical modeling, it is widely accepted that the interaction between the primary support and concrete lining can be modeled using Winkler springs (Vu and Broere 2018; Wood 2004). Duddeck (1979) proposed an idealized lining modeling that does not need to be circular for deep tunnels. According to the International Tunnelling Association Working Group on General Approaches to the Design of Tunnels (1988), noncircular cross-sections, like the horseshoe-shaped profile considered here, can therefore be taken into account as well (Möller 2006). A nonlinear finite-element program, ANSYS (ANSYS Inc. 2009), was employed to help understand the mechanical behavior of the tunnel lining mobilized by the monitored contact pressure. The numerical modelling is shown in Fig. 8, where the realistic lining of the horseshoe-shaped tunnel has non-uniform thickness (50 cm at the roof and 60 cm at the invert). Eight-node nonlinear SOLID 65 elements were used to simulate the tunnel lining because these allow for plastic deformation, cracking in tension, and crushing in compression and can adequately model the nonlinear behavior of the lining concrete in line with the Von Mises yield criterion (ANSYS Inc. 2009). In line with EN 1992-1-1 (2004), the Young's modulus and Poisson's ratio of the C30 concrete were assumed to be 33 GPa and 0.20, respectively.

Kolymbas (1998) proposed that the stiffness of a normal spring, K_s, normally positioned at the tunnel lining can be described by the expression:

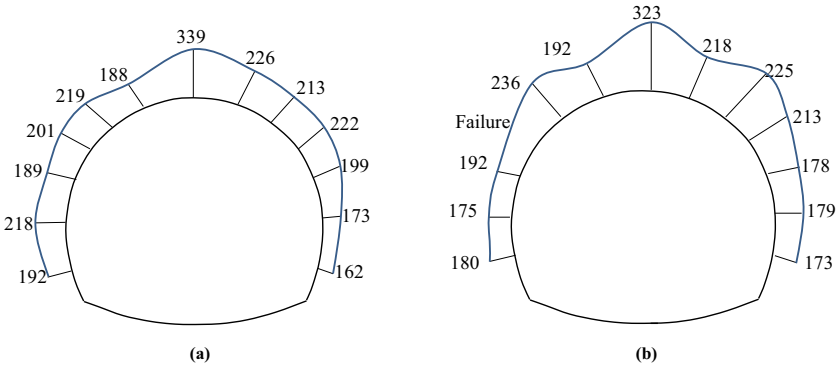

Fig. 6 Monitored ground loads acting on the primary support of Piaoli tunnel at Chainage: (a) YK6 + 955; (b) YK6 + 960 (all values are in kPa)

$$K_s = \frac{E(1-\nu)}{r(1+\nu)(1-2\nu)}, \quad (1)$$

where E is the Young's modulus, ν is the Poisson ratio of the ground, and r is the radius of the tunnel lining.

According to the experimental results of Clough and Duncan (1971), the shear stress acting on the interface between the tunnel lining and primary support is definitely less, and may be negligible, when compared with the normal stress. Therefore, in our numerical simulations, the compression-only elements (LINK10) were set normally on the tunnel lining to model the interaction between the primary support and tunnel lining (i.e., shear elements were omitted).

Figure 9 illustrates the principal stresses calculated for the tunnel lining. Interestingly, the most unfavorable position in the lining occurred at the roof. Note that positive values represent tension, and vice versa. The minimum stress σ_3 was approximately +1.75 MPa at the intrados of the roof in Fig. 9a, which did not exceed the tensile strength of C30 concrete (f_{ctm}), which was 2.90 MPa (EN 1992-1-1 2004). The maximum stress σ_1 was about −3.43 MPa at the extrados of the lining roof (Fig. 9b), which was much less than the compressive strength of C30 concrete (f_{ck}) of 30 MPa (EN 1992-1-1 2004).

Safety assessment of tunnel lining

Clearly, designing an NATM project necessitates consideration of the thrusts N and bending moments M acting on the lining structure (Evelyn 2017). Therefore, based on field-monitoring results obtained using the strain gauges, it was worthwhile discussing and assessing the safety of the tunnel lining. Before the cast-in-place lining was constructed, strain gauges were firmly fixed to the steel rebar (see Fig. 5c) to measure how much the strain changed in the reinforced lining when it was subjected to contact pressure.

Using the strain changes monitored at both the intrados and extrados of the tunnel lining, the thrust N and bending moment M can be respectively derived using the expressions:

Table 3 Components of monitored ground loads acting on primary support (all values are in kPa)

Position	Chainage		Mean	Ground load	Component	
	YK6 + 955	YK6 + 960			Vertical	Horizontal
Roof	339	323	331	331	331*	0
Above left hance	188	192	190	206	196	64*
Above right hance	226	218	222			
Left hance	219	236	228	223	180	131
Right hance	213	225	219			
Left springer	201	Failure	201	210	123	170
Right springer	222	213	218			
Above left side wall	189	192	191	190	59	181
Above right side wall	199	178	189			
Left sidewall	218	175	197	187	0	187
Right sidewall	173	179	176			
Left waist	192	180	186	177	55	168
Right waist	162	173	168			

*Note: the maximum vertical load, $q = 331$ kPa, occurred at the roof; the horizontal load of 64 kPa at the hance was equal to $0.2q$

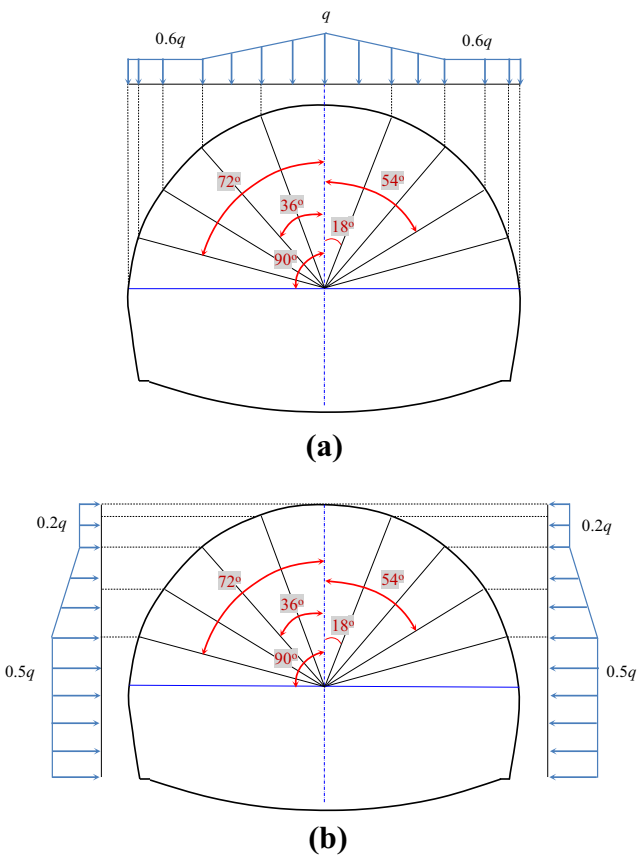

Fig. 7 Suggested profiles for the ground loads acting on the primary support of the horseshoe-shaped tunnel in highly weathered sandstone: (a) vertical component; (b) horizontal components. Note that q is 331 kPa in the current scenario

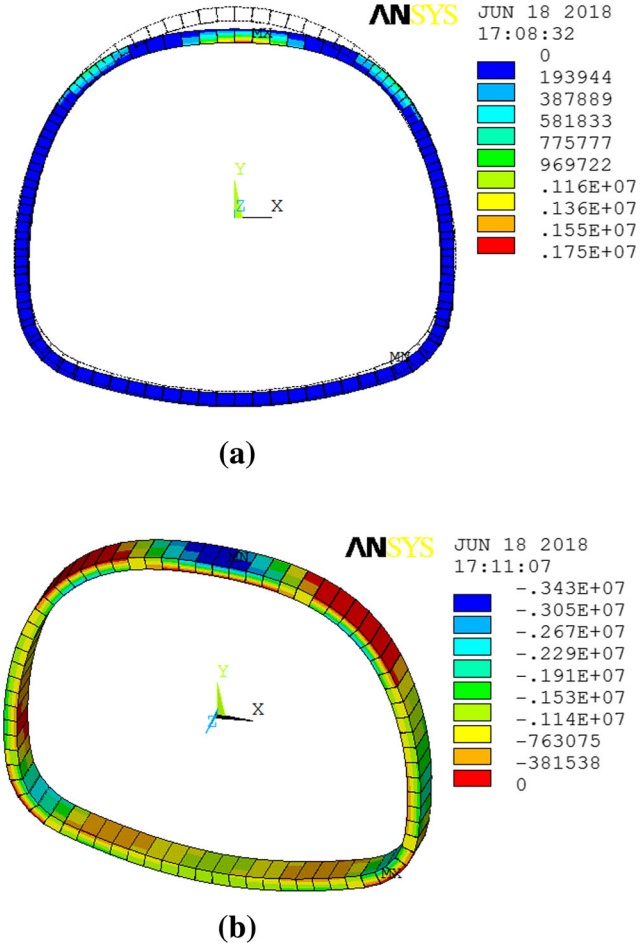

Fig. 9 Principal stress contours in the tunnel lining induced by contact pressure: (a) minimum stress σ_3; (b) maximum stress σ_1 (all values are in Pa). Positive stress represents tension; negative values signify compression

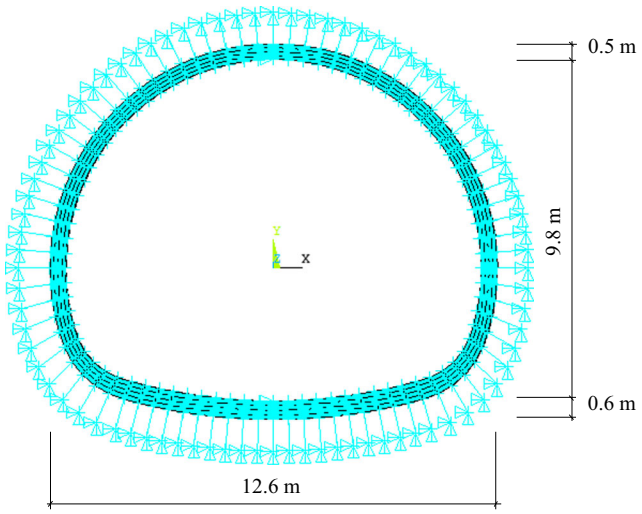

Fig. 8 Finite-element modeling used to characterize the structural responses of the horseshoe-shaped tunnel lining under field-monitored contact pressures. Note that compression-only elements (LINK10) were set normally on the tunnel lining, and the thickness of the lining was not uniform, i.e., 50 cm at roof and 60 cm at invert

$$\begin{cases} N = \dfrac{1}{2} \times E \times (\varepsilon_{\text{in}} + \varepsilon_{\text{ex}}) \times b \times h; \\ M = \dfrac{1}{12} \times E \times (\varepsilon_{\text{in}} - \varepsilon_{\text{ex}}) \times b \times h^2, \end{cases} \tag{2}$$

where ε_{in} and ε_{ex} refer to the strains (with signs) measured by the strain gauges embedded at the intrados and extrados of the tunnel lining, respectively, b denotes unit length along the tunnel axis (assumed to be 1 m here), and h signifies the thickness of the tunnel lining. Recall that the positive strain denotes tension, while the negative strain represents compression.

Using the strain-gauge measurements, the monitored axial thrust N and bending M for unit length along tunnel lining axis were calculated by means of Eq. (2) and are plotted in Fig. 10. The thrust distributions at the two chainages were somewhat similar, so only the results for Chainage YK6 + 955 are given here. Inspection of Fig. 10a reveals that the magnitude of the thrust on the lining roof

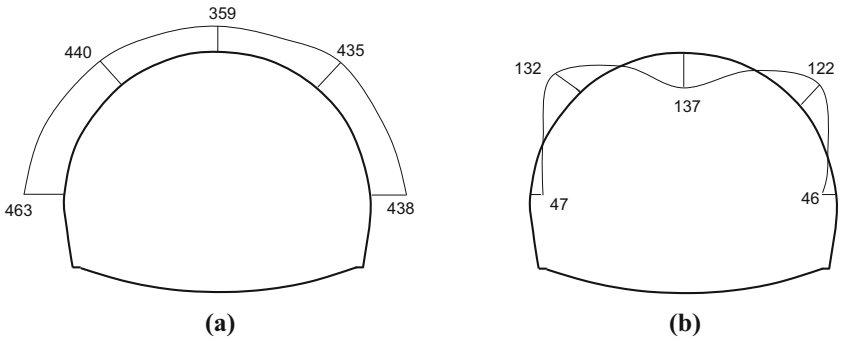

Fig. 10 Measured internal force profiles acting on the tunnel lining induced by contact pressure at Chainage YK6 + 955: (a) axial compressive thrust N (in kN); (b) bending moment M (in kN·m)

was slightly smaller than that at other positions, e.g., the sidewalls. The lateral thrust on the left was slightly greater than that on the right (463 kN on the left lining sidewall and 438 kN on the right, as opposed to 359 kN at the roof).

Figure 10b illustrates that the bending moments M took the form of a 'butterfly' shape. The maximum bending was quite appreciable (137 kN·m) at the roof of the tunnel lining and bent the lining inwards. The spandrels (located as in Fig. 4b), however, bent outwards with moments of 132 kN·m on the left and 122 kN·m on the right. Bending of the sidewalls was evidently much smaller, at 47 kN·m on the left and 46 kN·m on the right.

Figure 11a represents the cross-section of a lining member with typical strains and stress distributions for varying positions of the neutral axis (Mosley et al. 2007). The cross-section is subjected to bending moment M and axial compressive thrust N. The flowchart illustrated in Fig. 11b outlines the process used to assess whether the engineering structure is safe or not, according to Ultimate Limit States stipulated in EN 1992-1-1 (2004).

The location of the plastic centroid was determined by taking moments of all the stress resultants about an arbitrary axis, such as AA in Fig. 11a, so that:

$$\bar{x}_{\mathrm{p}} = \frac{\sum\left(F_{cc}h/2 + F_{sc}d' + F_{s}d\right)}{\sum\left(F_{cc} + F_{sc} + F_{s}\right)}, \tag{3}$$

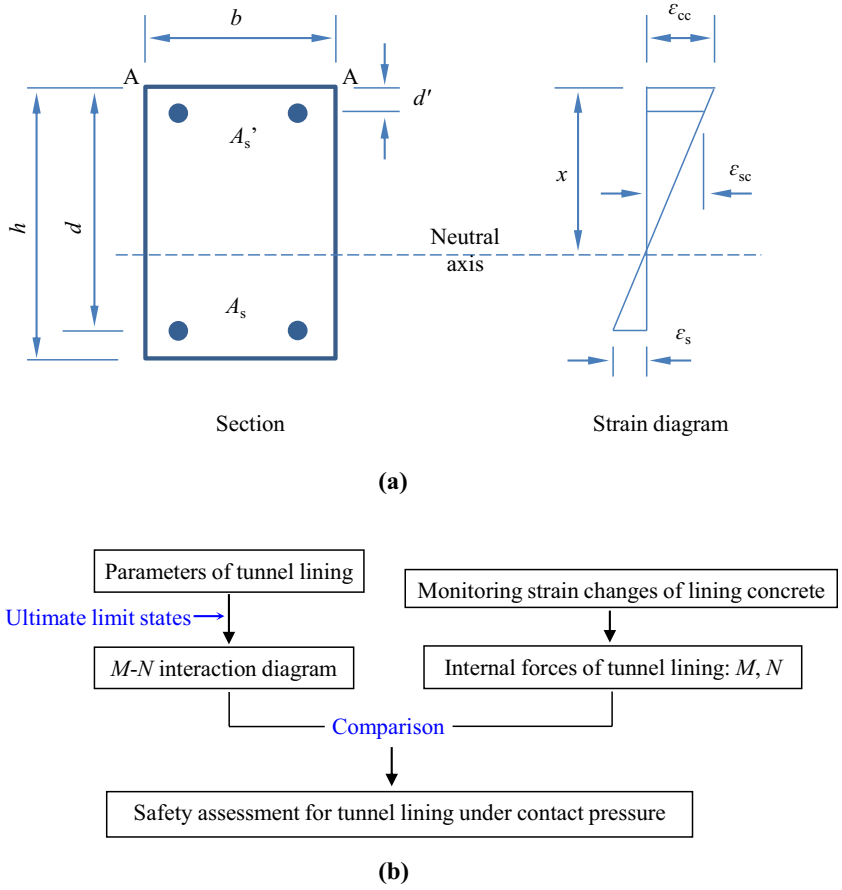

Fig. 11 Bending and axial thrust at the ultimate limit state: (a) symmetrical section of tunnel lining; (b) flowchart used to assess the safety of tunnel lining when subjected to contact pressure

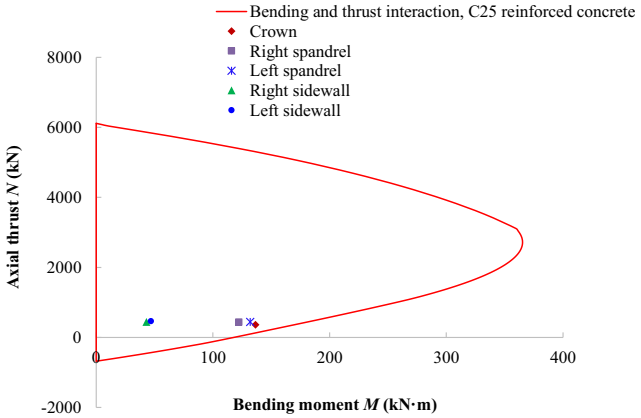

Fig. 12 Comparison of bending–thrust interaction diagram for tunnel lining cross-section with monitored internal forces at typical positions. The bending–thrust interaction diagram was calculated in terms of *Eurocode 2* (EN 1992-1-1 2004). Signs of bending need not be considered for the symmetrical section of the reinforced tunnel lining

where F_{cc} is the compressive force developed in the concrete and acting through the centroid of the stress block, F_{sc} is the compressive force in the reinforcement area $A_s^{'}$ and acting through its centroid, F_s is the tensile or compressive force in the reinforcement area A_s and acting through its centroid (EN 1992-1-1 2004; Mosley et al. 2007).

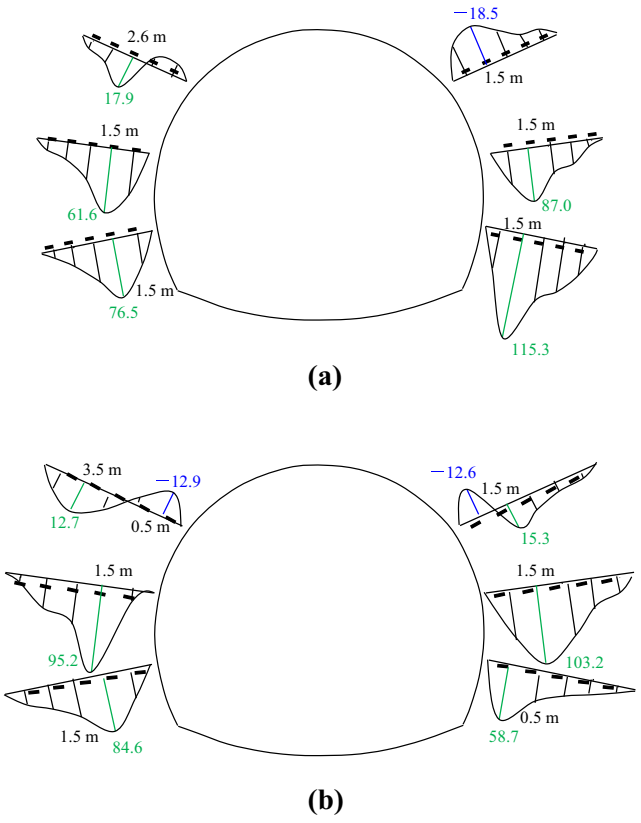

Fig. 13 Axial forces acting on the rockbolts in the highly weathered sandstone (unit: kN) for Chainages: (a) YK6 + 955; (b) YK6 + 960. A positive axial force denotes tension along the rockbolt axis, and vice versa

The applied force (N) must be balanced by the forces developed within the cross-section; therefore:

$$N = \begin{cases} 0.567 f_{ck} b \times 0.8x + f_{sc} A_s^{'} + f_s A_s & \text{if } 0.8x < h; \\ 0.567 f_{ck} bh + f_{sc} A_s^{'} + f_s A_s & \text{if } 0.8x \geq h, \end{cases} \quad (4)$$

where f_{ck} is the characteristic cylinder strength of concrete, f_{sc} is the compressive stress in steel area $A_s^{'}$, and f_s is the tensile or compressive stress in the reinforcement A_s (EN 1992-1-1 2004; Mosley et al. 2007).

Accordingly, the bending moment (M) about the plastic centroid is:

$$M = \begin{cases} 0.567 f_{ck} b \times 0.8x\left(\bar{x}_p - 0.8x/2\right) + f_{sc} A_s^{'}\left(\bar{x}_p - d^{'}\right) - f_s A_s\left(d - \bar{x}_p\right) & \text{if } 0.8x < h; \\ 0.567 f_{ck} bh\left(\bar{x}_p - h/2\right) + f_{sc} A_s^{'}\left(\bar{x}_p - d^{'}\right) - f_s A_s\left(d - \bar{x}_p\right) & \text{if } 0.8x \geq h, \end{cases} \quad (5)$$

By means of Eqs. (4) and (5), the bending–thrust interaction diagram corresponding to the Piaoli tunnel lining structure was plotted as the closed envelope curve shown in Fig. 12. Owing to the symmetry of the reinforced tunnel lining, the signs of bending did not need to be considered. Consequently, the monitored internal forces at typical positions of the Piaoli tunnel lining fell in the bending–thrust interaction diagram, suggesting that all monitoring positions were safe. In detail, the roof and spandrel had less safety margin and were closer to the envelope than that at sidewalls. This suggested that the steel rebars should be strengthened at both the intrados of the lining roof and extrados of the spandrels (for locations, see Fig. 4b). This would enhance the tensile strength of the lining in these regions (and thus their load-bearing capacity) in case an unexpected load is experienced. In contrast, the sidewall lining structures were considered safe, a result that compared well with field observations wherein no cracks could be found on the tunnel lining.

Axial forces on rockbolts

Rockbolts are typically capable of restraining large deformations and even preventing the collapse of a tunnel. During our field-monitoring campaign, due attention was focused on the non-uniform axial forces acting on the rockbolts around the tunnel boundary. This is reflected quite nicely by the results depicted in Fig. 13.

In this figure, a positive axial force (blue color) means tension along the rockbolts; conversely, a negative force (green color) implies compression. Indeed, all rockbolts in the springers and sidewalls are subject to tension and play a key role in restraining inward deformation of the tunneling periphery. Overall, the maximum tension eventually reached 115.3 kN near the right waist of Chainage YK6 + 955 (103.2 kN above the right sidewall of Chainage YK6 + 960). Moreover, the tension peaks about one-third to one-half of

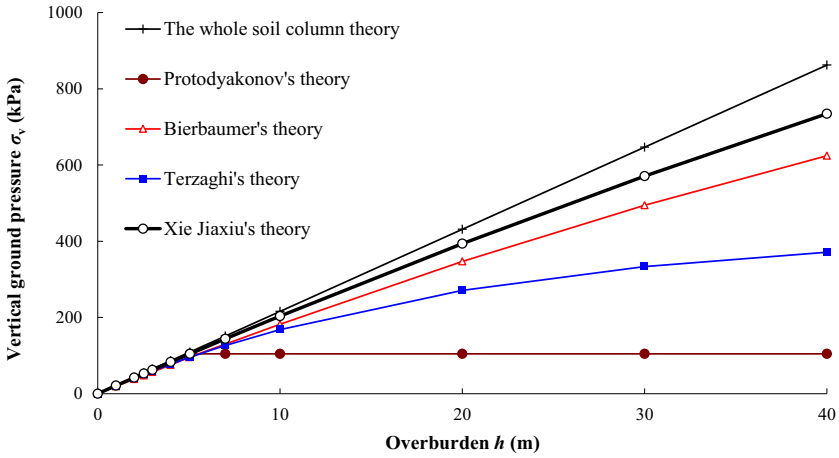

Fig. 14 Vertical ground loads σ_v on the tunnel structure, as calculated using various theories

Table 4 Comparison of vertical loads derived via field monitoring with those calculated using different theoretical methods

	Field value	Theoretical methods			
		Bierbaumer	Terzaghi	Protodyakonov	Xie Jiaxiu
Vertical load σ_v (kPa)	331	624	371	104	734
Theoretical/field ratio	–	1.89	1.12	0.31	2.22

the way along the bolts from their free ends at the periphery of opening were in good agreement with the neutral point theory proposed by Sun (1983).

Rockbolts above the hance, however, are subjected to compression, which is not beneficial to stabilizing the ground around the opening. This suggested that the rockbolts at the roof need to be replaced. In particular, field observations made on outcrops at the working faces of the tunnel revealed discontinuities developed in the rock mass in which the stability is expected to be controlled by the strength of the joints, i.e., cohesion and discontinuity friction. Therefore, it was concluded that the rockbolts at the roof should be substituted by pipe grouting work. This would enhance the reinforcement effect (Dalmalm 2004), as well as accelerate the construction schedule in practice.

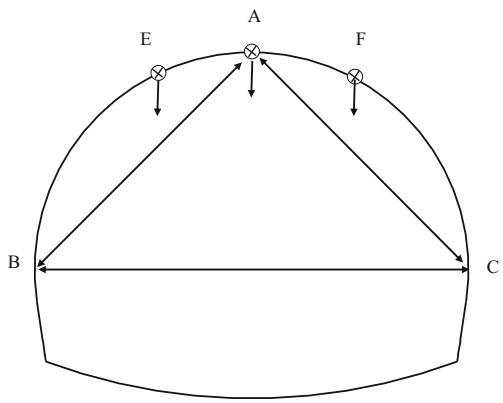

Fig. 15 Sketch of typical points used to monitor deformation around the tunnel periphery

Discussion

Comparison with typical theories

The theories that are typically used to calculate ground load in non-squeezing conditions are the whole-soil column theory, Bierbaumer's theory (Bierbaumer 1913), Xie Jiaxiu's theory (China Railway Eryuan Engineering Group 1997; Song et al. 2007), Protodyakonov's theory (Myrianthis 1975; Szechy 1970), and Terzaghi's theory (Terzaghi 1946). The basic principles underlying these theories are briefly described in Appendix A.

Recall that the span of the Piaoli highway tunnel is 12.6 m and its height is 9.8 m. Using the parameters in Table 1 along with the tunneling geometry, these theories were used to calculate the expected ground loads as a function of overburden depth. The results, shown in Fig. 14, revealed striking discrepancies between the different theories for this specific scenario. The whole-soil column theory predicted a linear increase in load as the depth of the tunnel increased, which seemed unacceptable for the deep tunnel considered here.

The theories of Xie Jiaxiu and Bierbaumer produced similar results, i.e., the magnitude of the ground load

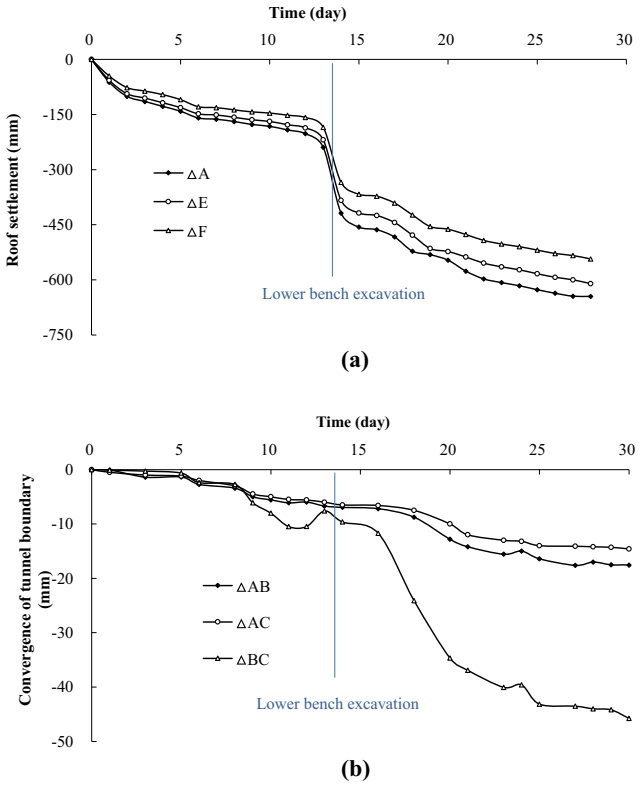

Fig. 16 Deformation (Δ) of the tunnel boundary at Chainage YK6 + 955 over a 30-day period: (a) roof settlement; (b) convergence of tunnel periphery

was virtually proportional to the overburden depth. The results generated using Terzaghi's theory appeared to be in line with our field-monitoring results (i.e., q = 331 kPa). Terzaghi (1946) hypothesized that the ground around the opening should be treated as a granular material (which is compatible with the highly weathered sandstone encountered herein) and assumed a slipping plane inclined at an angle of $(45° - \varphi/2)$ to the vertical (in the manner shown in Fig. 18). The ground load suggested by Protodyakonov's theory (104 kPa) was much less than those calculated by the theories (and field values) already discussed.

As detailed in Fig. 14, it is easy to compare the calculated vertical loads with data measured in the field (Table 4). Thus, the ground load found using Xie Jiexiu's theory was more than twice the field-monitoring value. The theoretical result calculated using Protodyakonov's theory was substantially less than the monitoring data and is unacceptable in tunnel design. However, the Bierbaumer and Terzaghi results were found to be close to the monitoring outcomes. In Bierbaumer's theory (Bierbaumer 1913), however, the vertical load on the tunnel structure increased with increasing buried depth (Fig. 14); hence, it might underestimate the arching effect acting on the surrounding rock above the roof of the tunnel lining, which acts to stabilize the tunnel itself.

Table 4 reveals that Terzaghi's theory can be used as a good proxy for predicting the peak magnitude of the vertical ground load acting on the structures of deep tunnels with large cross-sections passing through highly weathered sandstone. Additionally, it is worth noting that Terzaghi's theory of arching is valid for granular ground, rather than hard rock.

Deformation evolution

It is widely recognized that deformation of the tunnel is critical when assessing the stability of an excavation. To discuss deformation of the boundary of the Piaoli tunnel, monitoring points were installed, as shown in Fig. 15. Points A, E, and F are used to monitor the vertical settlement of the primary support at the roof; segments l_{AB}, l_{AC}, and l_{BC} monitor the convergence in the pertinent boundaries of the tunnel.

A non-contact technique was employed to derive the real-time evolution of the deformation of the tunnel boundaries over a 30-day monitoring period. The results are shown in Fig. 16. Considering the similarities between the two sections, only Chainage YK6 + 955 was selected here for analysis. The deformation of the tunnel boundary continuously increased, especially during excavation of the lower bench. It can be seen that the roof settled by

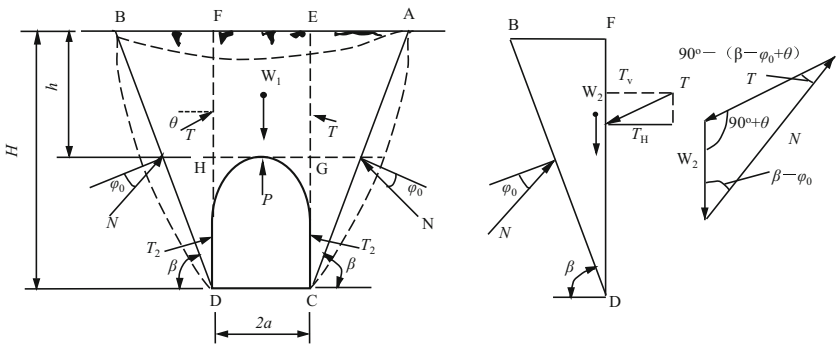

Fig. 17 Schematic diagram of the tunnel in Xie Jiaxiu's theory

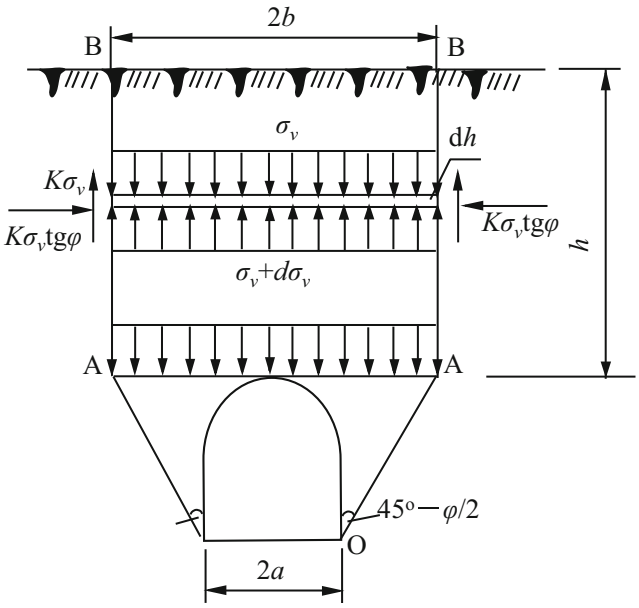

Fig. 18 Diagram illustrating the parameters involved in Terzaghi's theory

645 mm over the 30-day period (at point A); roof settlement dominated in this scenario. In contrast, the horizontal convergence between the sidewalls (l_{BC}) amounted to 43 mm over the same period. Therefore, to guarantee stability of the tunnel during construction, most attention should be devoted to monitoring deformation of the roof, specifically for the sudden increase in roof settlement expected to occur when the lower bench is excavated. The deformation of the tunnel boundary, which was recorded as a function of post-excavation duration, did not tend to level off. Thus, the cast-in-place C30 concrete lining needed to be constructed as soon as possible to prevent exaggerated tunnel deformation and, more importantly, to avoid the possibility of subsequent collapse.

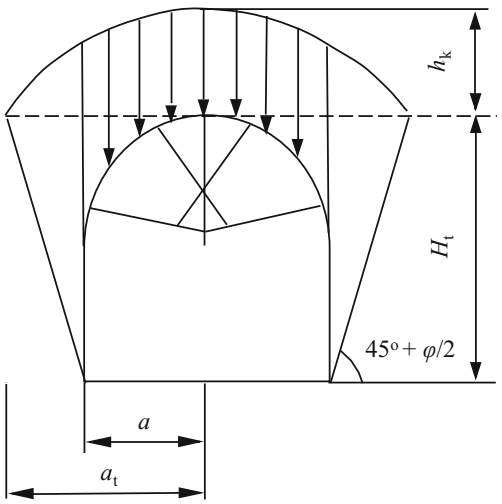

Fig. 19 Illustration showing the basis of Protodyakonov's theory

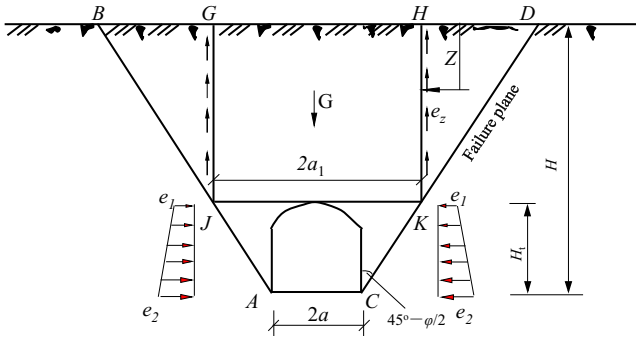

Fig. 20 Scheme used in Bierbaumer's theory

Conclusions

A systematic field-monitoring campaign was undertaken to investigate the ground loads on a tunnel structure, the behavior of the tunnel lining, the axial forces on the rockbolts, and deformation of the primary support. A tunnel driven through highly weathered sandstone was chosen, with the aim of improving current tunnel design practice for this commonly encountered type of rock mass.

- Based on the wealth of field data collected in highly weathered sandstone, the ground load acting on the tunnel structure did not conform to conventional specifications. The theory suggested by Terzaghi (1946) is capable of predicting the peak magnitude of the vertical ground load acting on a tunnel structure in highly weathered sandstone, but the results differ from those of field monitoring of the ground load profile.
- A potential profile for the ground load was proposed, in which the vertical load component is 'mountain'-shaped and the horizontal component adopts a 'folded-line' pattern. The peak of the vertical load (q) occurred at the roof of tunnel structure; it dropped linearly to $0.6q$ at the springer and then extended to the sidewall without change. The horizontal load was equal to $0.2q$ at the hance and increased linearly to $0.5q$ above the sidewall at an inclination of 72° from the vertical; it then remained unchanged to the tunnel invert.
- Rockbolts at the tunneling roof were subjected to compression when passing through highly weathered sandstone. These needed to be substituted by pipe grouting, which improves the reinforcement effect quite effectively and accelerates the construction schedule. In terms of deformation development around opening boundaries, settlement at the opening roof dominated when compared with horizontal convergence. As the Piaoli tunnel was constructed, more attention needed to be paid to roof settlement, especially during lower bench excavation.
- The bending moments acting on the tunnel lining adopted the shape of a butterfly. The maximum moment occurred

at the roof and corresponded to an inward bending; the moments at the spandrels corresponded to outward bending. According to Ultimate Limit States, it is therefore suggested that steel rebar be pre-installed at the intrados of the lining roof and the extradoses of the spandrels so as to enhance the tension capacity of the structure.

Acknowledgements This work was supported by the National Key Research and Development Program of China (Grant No. 2018YFC0407006) and the Young Scientists Fund of the National Natural Science Foundation of China (Grant No. 51809038). Two anonymous reviewers are thanked for critical reading of an early version of this paper and for their insightful comments. We thank Kathryn Sole, PhD, from Edanz Group (www.edanzediting.com/ac) for editing a draft of this manuscript.

Appendix A Theories typically used to calculate ground load

Whole-soil column theory

At shallow depths, the excavation-induced failure plane extends to the surface of the ground and frictional resistance is not considered. Consequently, the uniform vertical ground load q on the tunnel structure increases linearly with increasing buried depth:

$$q = \gamma h \tag{A1}$$

where γ denotes the unit weight of the ground and h represents the vertical distance from the ground surface to the tunnel roof.

Xie Jiaxiu's theory

The failure plane is assumed to be inclined at an angle β to the horizontal, as shown in Fig. 17. In this figure, the settlement of ground block GEFH (above the roof opening) would cause potential movement of lateral blocks FDB and ECA. According to Xie Jiaxiu's theory (China Railway Eryuan Engineering Group 1997; Song et al. 2007), the vertical ground load, q, can thus be expressed as:

$$\begin{cases} q = \gamma H\left(1-\dfrac{H}{2a}\lambda\tan\theta\right); \\ \lambda = \dfrac{\tan\beta-\tan\varphi_0}{\tan\beta[1+\tan\beta(\tan\varphi_0-\tan\theta)+\tan\varphi_0\tan\theta]}; \\ \tan\beta = \tan\varphi_0 + \sqrt{\dfrac{\sec^2\varphi_0\tan\varphi_0}{\tan\varphi_0-\tan\theta}}, \end{cases} \tag{A2}$$

where a is half the span of the excavation, λ is the lateral ground pressure coefficient (defined as the ratio of the horizontal to vertical ground loads) acting on the tunnel structure, β is the angle of inclination of the failure plane with respect to the horizontal direction, φ_0 is the computational friction angle, θ is the friction angle of the sliding surface l_{FH} or l_{EG}, and the other parameters are as previously defined.

Terzaghi's theory

Terzaghi (1946) assumed that the ground acts as a granular material. Thus, once the tunnel is excavated, the medium above the opening space is able to deform downwards. A sliding surface l_{OAB} is assumed to be formed (Fig. 18). Accordingly, Terzaghi found that the vertical ground pressure on the tunnel support is given by:

$$q = \frac{\gamma b}{\tan\varphi\cdot K}\left[1-\exp\left(-K\tan\varphi\cdot\frac{h}{b}\right)\right]. \tag{A3}$$

As the tunnel depth h increases, the second term in the square brackets gradually vanishes due to its exponential form, and Eq. (A3) simplifies to:

$$q = \frac{\gamma b}{\tan\varphi\cdot K} \tag{A4}$$

Protodyakonov's theory

This theory takes into consideration the arch effect hypothesized for deep tunnels, which leads to the formation of a parabolic profile above the tunnel roof (Myrianthis 1975; Szechy 1970). The weight of loose ground below the parabolic curve is referred to as the 'ground load' and is thus related to the dimensions of the tunnel (Fig. 19). The vertical ground pressure acting on the supporting structure is then calculated from the weight of the ground under the parabolic curve:

$$\begin{cases} a_t = a + H_t \times \tan(45-\varphi/2); \\ h_k = a_t/f = \dfrac{a_t}{(\tau/\sigma)} = a_t\cdot\sigma/(\sigma\tan\phi + c) = a_t/\tan\varphi; \\ q = \gamma \times h_k, \end{cases} \tag{A5}$$

where a_t is half the width of the collapse arch, a is half the span of the tunnel, H_t is the net height of the opening, φ is the friction angle of the ground, and h_k is the height of the collapse arch. It should be noted that the expressions in Eq. (A5) are not suitable for the condition where the buried depth of tunnel is less than five times the opening span ($10a$).

Bierbaumer's theory

Engineering practice shows that the ground load exerted on the structure of a tunnel is always less than the weight of the covering strata. By considering the forces of resistance (due to internal friction) and cohesion on the failure plane (Fig. 20), Bierbaumer (1913) theorized that the vertical load on the roof of the tunnel is:

$$q_b = \gamma H_t \left[1 - \frac{H_t}{2a_1} K_1 - \frac{c}{\gamma a_1}(1 - 2K_2)\right], \quad \text{(A6)}$$

where $a_1 = a + H_t \tan(45^\circ - \varphi/2)$, $K_1 = \tan\varphi \tan^2(45^\circ - \varphi/2)$, $K_2 = \tan\varphi \tan(45^\circ - \varphi/2)$.

References

Alija S, Torrijo FJ, Quinta-Ferreira M (2014) Study of the unexpected collapse of the Ampurdan tunnel (Spain) using a finite element model. Bull Eng Geol Environ 73:451–463. https://doi.org/10.1007/s10064-013-0534-z

ANSYS Inc. (2009) ANSYS user's manual revision 12.0. Canonburg, Pennsylvania, USA

Barton N, Lien R, Lunde J (1974) Engineering classification of rock masses for the design of tunnel support. Rock Mech 6:189–236. https://doi.org/10.1007/BF01239496

Bieniawski ZT (1973) Engineering classification of jointed rock masses. Trans S Afr Inst Civ Eng 15:335–344

Bierbaumer AH (1913) Die dimensionierung des tunnel manerwerks. Liepzig, Germany

China Railway Eryuan Engineering Group (1997) China railway design handbook: tunnel. China Railway Publishing House, Beijing

Clough GW, Duncan JM (1971) Finite element analyses of retaining wall behavior. J Soil Mech Found Div 97:1657–1673

Dalmalm T (2004) Choice of grouting method for jointed hard rock based on sealing time predictions. Dissertation. Royal Institute of Technology, Stockholm

Duddeck H (1979) Zu den berechnungsmethoden für die neue Österreichische tunnelbauweise. Rock Mech 3–27

EN 1992-1-1 (2004) Eurocode 2: Design of concrete structures - Part 1–1: General rules and rules for buildings. CEN, European Committee for Standardization, Brussels, Belgium

Evelyn OJ (2017) Geotechnical engineering design of a tunnel support system - A case study of Karuma (600 MW) hydropower project. Dissertation, University of Cape Town, South Africa

Goel RK, Jethwa JL, Dhar BB (1996) Effect of tunnel size on support pressure. Int J Rock Mech Min Sci Geomech Abstr 33:749–755

Gurocak Z (2011) Analyses of stability and support design for a diversion tunnel at the Kapikaya dam site, Turkey. Bull Eng Geol Environ 70:41–52. https://doi.org/10.1007/s10064-009-0258-2

Hatzor YH, He BG, Feng XT (2017) Scaling rockburst hazard using the DDA and GSI methods. Tunn Undergr Sp Technol 70:343–362. https://doi.org/10.1016/j.tust.2017.09.010

Hjálmarsson EH (2011) Tunnel support, use of lattice girders in sedimentary rock. MSc thesis, University of Iceland, Iceland

Hoek E, Brown ET (1997) Practical estimates of rock mass strength. Int J Rock Mech Min Sci 34:1165–1186. https://doi.org/10.1016/S1365-1609(97)80069-X

International Tunneling Association Working Group on General Approaches to the Design of Tunnels (1988) Guidelines for the design of tunnels. Tunn Undergr Sp Technol 3:237–249

JTG D70-2004 (2004) Code for design of road tunnel. China Communications Press, Beijing

Kim J, Kim J, Kim M, Yoo H (2015) Prediction of ground load by performing back analysis using composite support model in concrete lining design. KSCE J Civ Eng 19:1697–1706. https://doi.org/10.1007/s12205-015-1514-6

Kolymbas D (1998) Geotechnik – tunnelbau und tunnelmechanik. Springer, Berlin

Möller S (2006) Tunnel induced settlements and structural forces in linings. Doctoral Dissertation, University of Stuttgart, Germany

Mosley B, Bungey J, Hulse R (2007) Reinforced concrete design to Eurocode 2, 6th edn. Palgrave Macmillan, New York

Myrianthis ML (1975) Ground deformation associated with tunnelling and deep excavations in clay, with particular reference to London clay. Doctoral Dissertation, Durham University, United Kingdom

Rabcewicz L (1964) The new Austrian tunnelling method. Part I. Water Power 16:453–457

Rolf S, Alfred P, Zhang QW (2009) Design in tunnelling, structural design methods for the inner lining. Geomech Tunn 2:359–368. https://doi.org/10.1002/geot.200900027

Simanjuntak TDYF, Marence M, Mynett AE, Schleiss AJ (2014) Pressure tunnels in non-uniform in situ stress conditions. Tunn Undergr Sp Technol 42:227–236. https://doi.org/10.1016/j.tust.2014.03.006

Singh B, Goel RK, Jethwa JL, Dube AK (1997) Support pressure assessment in arched underground openings through poor rock masses. Eng Geol 48:59–81

Song YX, Jia XY, Zhu YQ (2007) Study on vertical earth pressure calculation of metro tunnel. Rock Soil Mech 28:2240–2244

Sun XY (1983) Grouted rock bolt used in underground engineering in soft surrounding rock or in highly stressed regions. In: Stephansson O (ed) Proceedings of the international symposium on rock bolting. Abisko, pp 345–352

Szechy K (1970) The art of tunnelling. Akademiai Kaido, Budapest

Taromi M, Eftekhari A, Hamidi JK, Hamidi A (2017) A discrepancy between observed and predicted NATM tunnel behaviors and updating: a case study of the Sabzkuh tunnel. Bull Eng Geol Environ 76:713–729. https://doi.org/10.1007/s10064-016-0862-x

Terzaghi K (1943) Theoretical soil mechanics. Wiley, New York

Terzaghi K (1946) Introduction to tunnel geology in rock tunneling with steel supports. Youngstown, Ohio, USA

Vu MN, Broere W (2018) Structural design model for tunnels in soft soils: from construction stages to the long-term. Tunn Undergr Sp Technol 78:16–26. https://doi.org/10.1016/j.tust.2018.04.017

Wood DM (2004) Geotechnical modelling. CRC Press, Boca Raton

Zhang DL, Fang Q, Li PF, Wong LNY (2013) Structural responses of secondary lining of high-speed railway tunnel excavated in loess ground. Adv Struct Eng 16:1371–1379. https://doi.org/10.1260/1369-4332.16.8.1371